Time Resolved SAXS and RNA Folding

Lois Pollack
School of Applied and Engineering Physics, Cornell University, Ithaca, NY 14853

Received 30 November 2010; revised 19 January 2011; accepted 19 January 2011
Published online 15 February 2011 in Wiley Online Library (wileyonlinelibrary.com). DOI 10.1002/bip.21604

ABSTRACT:

Small angle X-ray scattering provides low resolution structural information about macromolecules in solution. When coupled with rapid mixing methods, SAXS reports time-dependent conformational changes of RNA induced by the addition of Mg^{2+} to trigger folding. Thus time-resolved SAXS provides unique information about the global or overall structures of transient intermediates populated during folding. Notably, SAXS provides information about the earliest folding events, which can evade detection by other methods. © *2011 Wiley Periodicals, Inc. Biopolymers 95: 543–549, 2011.*

Keywords: RNA folding; small angle X-ray scattering; ion-nucleic acid interactions

This article was originally published online as an accepted preprint. The "Published Online" date corresponds to the preprint version. You can request a copy of the preprint by emailing the Biopolymers editorial office at biopolymers@wiley.com

SAXS BACKGROUND

Small angle X-ray scattering provides global structural information about macromolecules in solution.[1,2] When coupled with experimental methods that trigger conformational changes, e.g., by modifying the solvent through mixing, SAXS reports time-dependent structural changes. Time-resolved SAXS has been applied to study protein folding,[3–17] DNA compaction,[18] protein conformational dynamics,[19] and the topic of this contribution, RNA folding.[20–26] The RNA folding problem continues to gain visibility with the increasing recognition of RNA's importance to cellular biology. Folding into specific three-dimensional structures enables RNA involvement in processes including splicing,[27] gene regulation,[28] or the assembly of ribo-nucleoprotein machines.[29,30] The application of time-resolved SAXS to this problem offers the unique opportunity to monitor both the large and small scale structural changes that accompany RNA tertiary structure acquisition.

Small angle scattering from a macromolecule occurs when electrons within the molecule are excited by the electric field of the incident X-ray beam. Each electron re-radiates or scatters the beam. Phase differences arise between waves scattered by electrons at different positions within the sample (Figure 1). The total scattering amplitude is computed at each scattering angle 2θ by adding the amplitude of all scattered waves, while carefully accounting for phase differences between them. As intensity (not amplitude) is measured by detectors, the scattering profile is the product of the amplitude and its complex conjugate. This measurement also reflects the orientational average of macromolecules in solution relative to the direction of the incident beam.

Scattering profiles are typically recorded as images on area detectors. The intensity of radiation scattered into an angle 2θ is determined by integrating over all of the pixels in the image at this angle, e.g., in a circle of fixed radius around the beam center. Figure 1 suggests how one-dimensional scattering profiles are derived from images. Scattering intensity is usually plotted as a function of the momentum transfer $q = 4\pi\sin\theta/\lambda$ where θ is half the scattering angle and λ is the X-ray wavelength.

Scattering profiles contain a great deal of useful information about macromolecular structure.[1,2] The intensity of radiation scattered into the forward angle, at $q = 0$ (equivalently $\theta = 0$) known as $I(0)$ or I_0 is proportional to the molecular weight of the macromolecule. Changes in I_0 provide a useful control for (unintentional) molecular association that sometimes accompanies folding because of the high RNA concentrations required for some experiments: a few mg ml^{-1}. At angles just above zero, the Guinier approximation can be used to extract the molecular radius of gyration, R_g, the mean square distance between pairs of electrons in the sample. At these low angles (corresponding to $q < 1.3/R_g$) the scattering

Correspondence to: Lois Pollack; e-mail: lp26@cornell.edu
©2011 Wiley Periodicals, Inc.

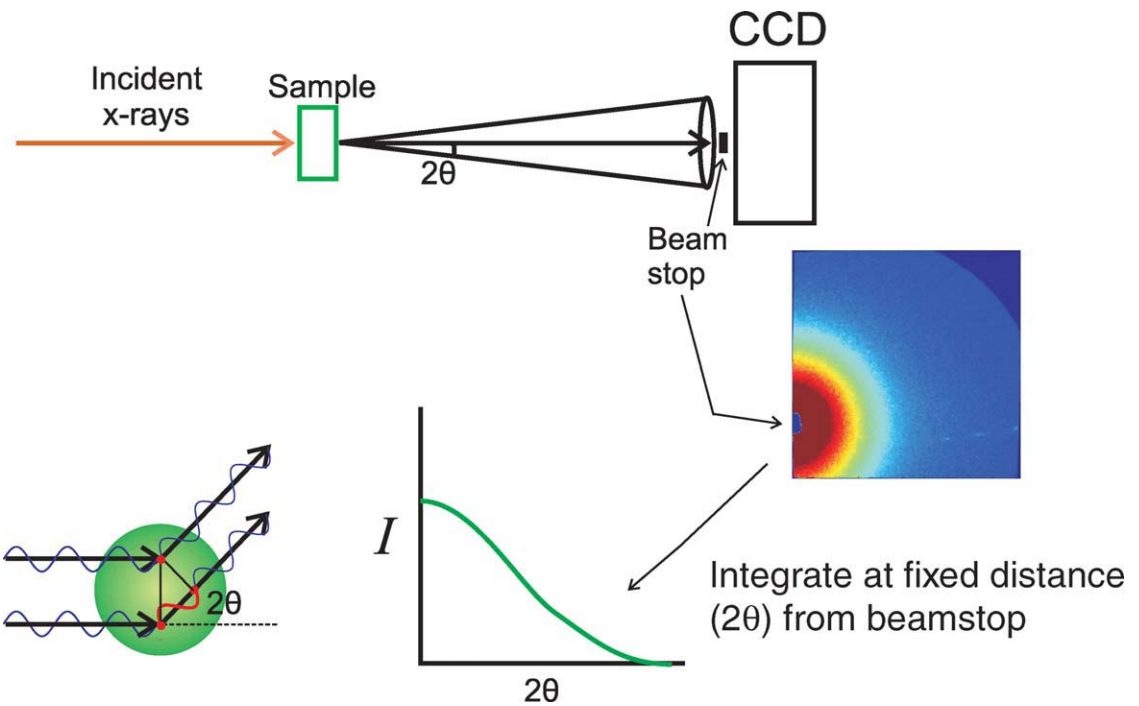

FIGURE 1 A schematic of a SAXS experiments is illustrated, showing the scattering geometry. The scattered radiation is collected on a CCD detector and displayed as an image. The image is converted into a scattering profile by integrating the counts at fixed distances from the beamstop, corresponding to different scattering angles, 2θ. The scattering profile reflects phase differences between X-rays scattered from different positions within the sample (green circle, lower left). The two scattered waves pictured here display a phase difference of 2π radians (equivalent to one full wavelength).

profile is modeled as a Gaussian whose width is related to $R_g^2/3$. R_g is a useful measure of molecular size during the earliest stages of folding; it can vary dramatically as molecular states change from extended to compact (see for example Figure 2). Changes in $I(q)$ at larger q reflect the compactness of the structure. Kratky plots of $I(q^2)$ vs. q are useful for interpreting data in this regime[1]; multiplication by q^2 enhances data at large relative to low q. In this mid-q range, a broad peak in the Kratky plot signifies molecular compaction; in contrast Kratky plots of extended states tend to increase with q in this angular range (see Figure 3). Data acquired at high q report on length scales below ~20 Å. Here, scattering profiles reflect molecular details like the helical diameter, and may converge for unfolded and folded molecules.

Full SAXS profiles can be analyzed to extract more detailed structural information.[31] Fourier transforms of $I(q)$ yield pair distance distribution functions $P(r)$ which provide insight into the real space distribution of electrons within the macromolecule. The $P(r)$ curves corresponding to unfolded vs. folded states reflect the different pairwise distances found in each ensemble.[31,32] Full scattering profiles

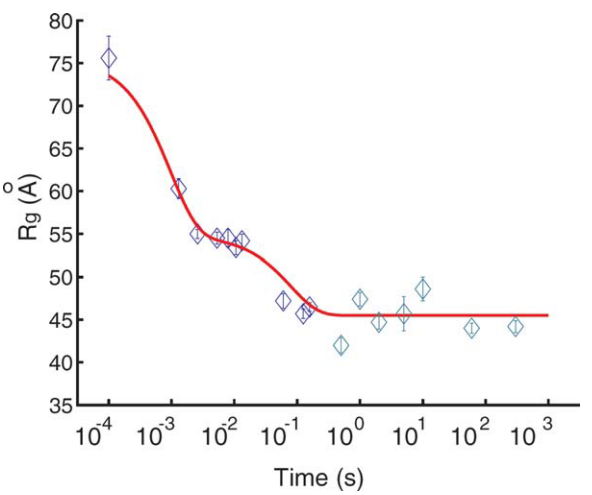

FIGURE 2 A plot of molecular radius of gyration, R_g, of the wild-type *Tetrahymena* ribozyme as a function of time after initiation of folding following the addition of 10 m*M* Mg^{2+}. The leftmost point corresponds to the Mg^{2+}-free state. Two distinct phases are measured. The blue (green) symbols correspond to data acquired by continuous (stopped) flow mixing. The red line is the best fit to a two exponential function following Kwok et al., J Mol Biol 2006.

10970282, 2011, 8, Downloaded from https://onlinelibrary.wiley.com/doi/10.1002/bip.21604 by Cornell University, Wiley Online Library on [28/06/2023]. See the Terms and Conditions (https://onlinelibrary.wiley.com/terms-and-conditions) on Wiley Online Library for rules of use; OA articles are governed by the applicable Creative Commons License

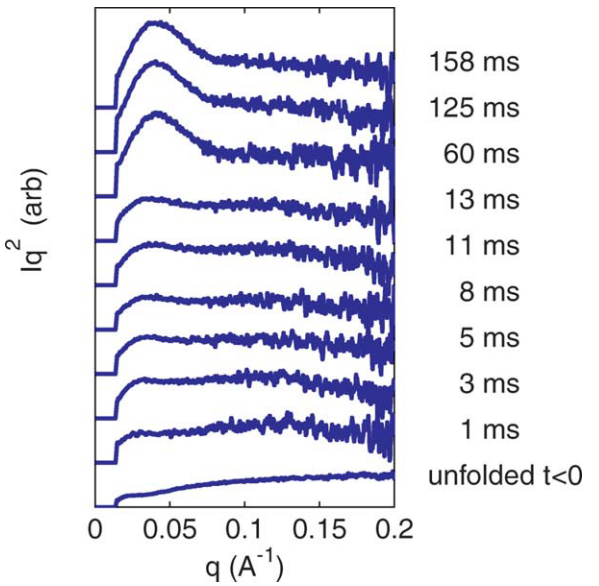

FIGURE 3 Multiplication of scattering intensity I by q^2 (a Kratky plot), emphasizes the shape of the scattering profile at q values larger than those used to compute R_g. Kratky plots for dataset of Figure 2 are shown as a function of time after mixing in milliseconds, beginning with unfolded RNA (bottom curve). The curves are offset for display purposes. The appearance of a well-defined peak indicates significant molecular compaction.

can also be used in conjunction with singular value decomposition algorithms to identify the appropriate number of principal components required to generate a set of related curves.[33,34] When applied to time-resolved data, this approach provides reaction kinetics in addition to structural information about intermediates. Another approach employs reconstruction algorithms[35–38] that provide plausible low resolution structural envelopes suggesting actual macromolecular conformations. A recent review summarizes many of the resources available for SAXS reconstructions.[39] These algorithms have successfully been applied to reconstruct homogeneous populations of molecules in equilibrium. Reconstructions of transient states, although intriguing in theory, must be carefully interpreted, as discussed in Ref. 40.

In summary, SAXS provides low resolution structural information about macromolecules in solution. Both reaction kinetics and time-dependent structures can be extracted from SAXS data. The challenges associated with time-resolved SAXS studies of RNA folding arise from the complexity of the process itself.[41] Parallel pathways have been observed,[23,42] long lived misfolded states[41,43] can coexist with properly folded molecules and multiple interconverting native states can exist.[44] Dimerization can also occur at mg ml^{-1} concentrations.[26] In spite of these challenges, the information provided by time-resolved SAXS is unique and informative.

Experimental Considerations for Time-Resolved SAXS

SAXS signal strength depends on many variables including the "contrast" or electron density difference between RNA and solvent. Although RNA's electron density is nearly twice that of water,[45] it is composed of low atomic number elements. Thus the absolute signal strength is moderate, since it is proportional to the number of excess electrons relative to the bulk solvent. High signal to noise requires intense X-ray beams from synchrotron sources. Signal strength scales with X-ray exposure time, with the volume of (illuminated) sample, and with macromolecule concentration. These parameters are all subject to practical limits. Long exposure times or high beam intensities result in radiation damage; high nucleic acid concentrations can lead to dimerization. If folding is initiated by the addition of Mg^{2+} to a solution containing RNA at low ionic strength, the time scale for mixing increases with the volume of sample to be mixed. Experimental parameters must be carefully optimized to obtain sharp time resolution.

The first time-resolved SAXS studies of RNA folding were carried out by Russell et al.[24] The Group I intron from *Tetrahymena* was prepared in low ionic strength buffer containing only monovalent cations. A Mg^{2+}-containing solution was added by hand to initiate folding. SAXS profiles measured before and ~1 min after mixing with Mg^{2+} displayed dramatic differences and motivated the application of more sophisticated methods to the problem. Comparable manual mixing techniques have also been used to study folding of the catalytic domain of *Bacillus subtilis* RNAse P RNA (C-domain RNA).[21]

Most rapid mixing experiments rely on either stopped or continuous flow mixer technology.[34] In stopped flow experiments, two solutions are rapidly injected through a mixing chamber into an observation chamber. The flow is stopped to contain the sample within this chamber and measurements are acquired as a function of real time. Stopped flow mixers have many advantages for SAXS experiments. Since the cross section of the beam can be as large as the sample cell, a large beam area can be employed, boosting signal strength. Newer mixers achieve submillisecond mixing times when micro-volume attachments to commercially available devices are used.[23] An increased variety of "final" conditions can be achieved if the mixer can accommodate multiple syringes whose contents are mixed in different ratios. Measurements can also be acquired at long times after mixing is

10970282, 2011, 8, Downloaded from https://onlinelibrary.wiley.com/doi/10.1002/bip.21604 by Cornell University, Wiley Online Library on [28/06/2023]. See the Terms and Conditions (https://onlinelibrary.wiley.com/terms-and-conditions) on Wiley Online Library for rules of use; OA articles are governed by the applicable Creative Commons License

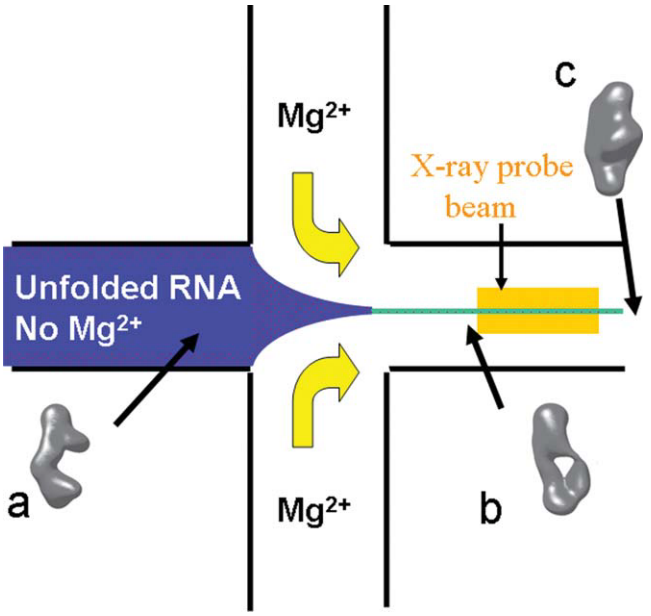

FIGURE 4 A cartoon of an RNA folding experiment using the continuous flow mixing method described in the text. Folding is initiated within the microfabricated flow cell by the rapid addition of Mg^{2+} ions. The RNA folds as it flows down the channel; the X-ray beam can be moved to probe the conformation at any position in the flow cell. Reconstructions of scattering profiles (from Lamb et al., J Appl Cryst 2008) are shown at different locations along the channel to indicate potential molecular structures.

complete. The disadvantages of stopped flow include limitations on exposure times, especially when measuring the most rapid events, and on solution conditions since mixing is always accomplished by dilution. Some sample is always "wasted" because the beam cannot fill the entire sample cell. Finally, a "stopped" or immobile sample is subject to radiation damage which may become severe for long beam exposures or high X-ray intensity.

Continuous flow mixers have also been used to study folding reactions. In these mixers (shown in Figure 4), mixing is achieved by the rapid diffusion of small salt ions from the side to the center channel.[46,47] Time resolution is achieved by measuring at different locations along the outlet channel; each position corresponds to a fixed time after mixing. The advantages of this technology result from the flow itself. The sample is very efficiently used: every molecule that travels down the channel contributes to the signal. Flow also eliminates concerns about radiation damage. A broad range of reaction conditions is available by changing the composition of the fluids in the side channels. Finally, since mixing follows from diffusion not dilution, for short times, where the diffusion of RNA is negligible, the RNA concentration is always the same, regardless of reaction conditions. Using improved versions of the mixer,[47] it is possible to achieve mixing (and measurement) times as short as 0.1 ms. The main disadvantage of this technology is the need for very small, stable X-ray beams.[12] However, given the high quality of current X-ray sources (and planned next generation sources) beam stability is no longer an issue. It is a challenge to measure on long time scales (longer than ~1 sec after mixing) because the diffusive broadening of the RNA-containing jet leads to sample concentrations that change with time (position along the channel).[22]

Both continuous and stopped flow were applied[25] to fill in the "dead time" of the manual mixing experiments described above. The time resolution of the stopped flow mixers employed for these studies was of order 10s of msec. Time scales beginning on the single millisecond were accessible via continuous flow. This combination of technologies was used to monitor folding of the *Tetrahymena* ribozyme and several carefully selected mutants.[20,22,25,26] Most recently, stopped flow mixing with a micro-volume mixer head has been applied to study folding of the *Azoarcus* ribozyme.[23] Results of these studies will be discussed in the next section.

Results of Time Resolved SAXS Experiments Studying RNA Folding

The first RNA folding experiment probed the time-dependent radius of gyration of the *Tetrahymena* ribozyme following manual mixing with Mg^{2+}.[24] During the 1-min experimental deadtime, the R_g decreased from 74 Å in the initial, low salt state, to 51 Å in Mg^{2+}. This important experiment demonstrated the formation of compact states following the addition of Mg^{2+} to induce tertiary structure formation.

Follow-up experiments probed ribozyme folding on shorter time scales, using both continuous and stopped flow mixers.[25] Scattering profiles were acquired 5 ms to 1000 s after the addition of Mg^{2+}. Singular value decomposition was used to identify the smallest number of independent curves required to span (recreate) all of the time dependent curves.[34] Each time-dependent curve was projected onto these basis states and time-dependent changes in these projection coefficients reported the kinetics of folding. These experiments were the first to demonstrate structural changes within milliseconds of the addition of Mg^{2+}. Additional discrete kinetic phases follow this initial rapid change. To interpret the rapid collapse, comparison was made with data from time-resolved hydroxyl radical footprinting experiments. This latter method monitors the formation of individual tertiary contacts during Mg^{2+} induced folding.[48] The footprinting experiments of Ref. 48 were carried out at higher temperature and lower initial ionic strength than the SAXS experiments, but reported no changes in tertiary contact formation on the time scale of the initial collapse. Taken

10970282, 2011, 8, Downloaded from https://onlinelibrary.wiley.com/doi/10.1002/bip.21604 by Cornell University, Wiley Online Library on [28/06/2023]. See the Terms and Conditions (https://onlinelibrary.wiley.com/terms-and-conditions) on Wiley Online Library for rules of use; OA articles are governed by the applicable Creative Commons License

together these data suggested that collapse precedes tertiary contact formation. These results focused attention on the role of tertiary contact formation in molecular compaction.

Follow-up experiments[20] explored the role of tertiary contact formation in compaction and folding of this ribozyme. Five long-range tertiary contacts were eliminated by mutation. Folding of this construct was followed with SAXS using both continuous and stopped flow mixing. Principal component analysis revealed that the first phase of collapse persists even in the absence of these key tertiary contacts. This initial collapse can be induced by the addition of either 10 m*M* Mg^{2+} or 1 *M* Na^{+}. Based on these observations, the most rapid collapse was linked to the reduction of strong electrostatic repulsion between duplexes that exists at the low ionic strength of the initial buffer, e.g., when the screening length far exceeds the distance between helices.

Subsequent experiments employed concordant time resolved SAXS and footprinting to monitor collapse and tertiary contact formation.[22] Experimental conditions were matched as closely as possible within the differing constraints of the two technologies: the initial concentration of monovalent salt, as well as temperature was identical. These experiments probed the compaction and folding of the wild-type ribozyme, and several mutants in which groups of contacts were selectively knocked out. Interestingly, no significant changes in protections were measured by footprinting during the initial phase measured by SAXS; however, subsequent compaction (signaled by SAXS) occurred on the same time scale as contact formation (signaled by footprinting). Notably, the formation of contacts within the fastest folding, P4-P6 domain is coincident with the second compaction phase measured by SAXS in the full length construct on a time scale of ~100 ms. These results are consistent with electrostatic relaxation due to the more localized screening of (highly-charged) RNA backbone in Mg^{2+} as opposed to in low ionic strength solutions containing monovalent ions alone. Reduction of inter-helix (electrostatic) repulsion as ionic strength is increased is evident from measurements of the second virial coefficients of short RNA duplexes as a function of ionic strength[49]; however other factors may also contribute to this reduction in size.

Additional coupled SAXS and footprinting experiments probed the independently-folding P4-P6 domain.[26] P4-P6 folding occurs with a time constant of ~10 ms. Two constructs were studied: wildtype P4-P6 and a mutant in which stabilizing tertiary contacts were knocked out. No changes to SAXS profiles of either construct were measured immediately after the addition of Mg^{2+} to initiate folding, suggesting that the molecule remains in extended conformations. In the wild-type domain, on longer time scales, compaction (reported by SAXS) is accompanied by tertiary contact formation (reported by footprinting). The absence of millisecond scale electrostatic relaxation suggests that additional barriers to folding may exist, such as the ionic-strength-dependent flexibility of hinges joining the two parts of this domain. The importance of flexible, non-base-paired regions in directing the formation of RNA structures has been noted in the literature.[50]

Time-resolved SAXS has also been used in conjunction with other biochemical techniques, most notably time-resolved fluorescence and absorption spectroscopies, to monitor folding of C-domain RNAse P RNA.[21] Folding to the native structure is initiated by the addition of cations to RNA in low ionic strength solution. This domain folds through a series of sequentially populated intermediates; no evidence for non-native structures has emerged. Such a straightforward reaction scheme considerably simplifies the interpretation of time-resolved SAXS experiments and, in conjunction with information available from other methods,[51] allows determination of the rate limiting step for C-domain folding. Two discrete steps are reported by SAXS: a rapid compaction is followed by more subtle structural changes consistent with rearrangements of an already compact structure around prebound metal ions.

Most recently, time-resolved SAXS has been applied to study folding of the *Azoarcus*[23] Group I ribozyme, which is smaller and structurally simpler than the *Tetrahymena* ribozyme.[52] Micro-liter volume stopped flow mixing was employed in conjunction with rapid detectors to monitor folding with submillisecond time resolution. Experimental results are described by a model in which parallel and Mg^{2+} concentration dependent folding pathways exist. Following charge compensation on a local scale, folding can be rapid (and correct) if the molecule collapses to a conformation that enables native contact formation. However a detailed analysis of the data suggests that not all molecules follow this direct pathway. Parallel pathways contribute if non-native contacts are present in the unfolded state,[43] or form in compact intermediates.[41]

SUMMARY AND CONCLUSION

SAXS provides information about the structure of transient intermediates populated during folding and as such is a valuable probe of folding. SAXS readily distinguishes extended from compact states, and partially (e.g., intermediate) from very (e.g., native) compact states. The dramatic conformational changes accompanying the former transition are easily measured with SAXS and can be time-resolved in conjunction with rapid mixing and/or detection methods. The latter

10970282, 2011, 8, Downloaded from https://onlinelibrary.wiley.com/doi/10.1002/bip.21604 by Cornell University, Wiley Online Library on [28/06/2023]. See the Terms and Conditions (https://onlinelibrary.wiley.com/terms-and-conditions) on Wiley Online Library for rules of use; OA articles are governed by the applicable Creative Commons License

class of transitions can also be probed by SAXS and benefit from direct comparison with time-resolved data acquired by other methods with comparable time resolution (time-resolved footprinting,[53] fluorescence spectroscopies,[54,55] or on longer time scales, time-resolved NMR[56]). Thus the great strength of SAXS lies in its ability to monitor even subtle structural changes under a variety of different solution conditions, with time resolution as sharp as submillisecond. The great weakness of SAXS is that it is an ensemble measurement. This weakness is amplified by the very nature of RNA folding which sometimes exploits parallel and/or nonproductive folding pathways. Interpretation of measurements of such heterogeneous ensembles can be extremely challenging. Future applications of time-resolved SAXS have the potential to provide new information about the nature of the initial compaction, specifically by identifying arrangements of rigid helical elements consistent with the overall dimensions of transient structures. These experiments will require sharper, microsecond scale time resolution. Other potentially exciting applications include following the dynamics of riboswitches in action.[57]

In spite of the complexities and challenges associated with time-resolved SAXS, it is one of the few techniques that provide the size and shape of transient structures to complement the information available from other probes of folding.

REFERENCES

1. Glatter, O. Small Angle X-Ray Scattering; Academic Press: London, 1982.
2. Guinier, A.; Fournet, G. Small-Angle Scattering of X-Rays; Wiley: New York, 1955.
3. Akiyama, S.; Takahashi, S.; Kimura, T.; Ishimori, K.; Morishima, I.; Nishikawa, Y.; Fujisawa, T. Proc Natl Acad Sci USA 2002, 99, 1329–1334.
4. Arai, M.; Ikura, T.; Semisotnov, G. V.; Kihara, H.; Amemiya, Y.; Kuwajima, K. J. Mol Biol 1998, 275, 149–162.
5. Chen, L. L.; Wildegger, G.; Kiefhaber, T.; Hodgson, K. O.; Doniach, S. J Mol Biol 1998, 276, 225–237.
6. Eliezer, D.; Chiba, K.; Tsuruta, H.; Doniach, S.; Hodgson, K. O.; Kihara, H. Biophys J 1993, 65, 912–917.
7. Kim, S. J.; Matsumura, Y.; Dumont, C.; Kihara, H.; Gruebele, M. Biophys J 2009, 97, 295–302.
8. Kuwajima, K.; Arai, M.; Inobe, T.; Ito, K.; Nakao, M.; Maki, K.; Kamagata, K.; Kihara, H.; Amemiya, Y. Spectrosc Int J 2002, 16, 127–138.
9. Matsumura, Y.; Shinjo, M.; Mahajan, A.; Tsai, M. D.; Kihara, H. Biochimie 2010, 92, 1031–1039.
10. Plaxco, K. W.; Millett, I. S.; Segel, D. J.; Doniach, S.; Baker, D. Nat Struct Biol 1999, 6, 554–556.
11. Pollack, L.; Tate, M. W.; Darnton, N. C.; Knight, J. B.; Gruner, S. M.; Eaton, W. A.; Austin, R. H. Proc Natl Acad Sci USA 1999, 96, 10115–10117.
12. Pollack, L.; Tate, M. W.; Finnefrock, A. C.; Kalidas, C.; Trotter, S.; Darnton, N. C.; Lurio, L.; Austin, R. H.; Batt, C. A.; Gruner, S. M.; Mochrie, S. G. J Phys Rev Lett 2001, 86, 4962–4965.
13. Segel, D. J.; Bachmann, A.; Hofrichter, J.; Hodgson, K. O.; Doniach, S.; Kiefhaber, T. J Mol Biol 1999, 288, 489–499.
14. Segel, D. J.; Eliezer, D.; Uversky, V.; Fink, A. L.; Hodgson, K. O.; Doniach, S. Biochemistry 1999, 38, 15352–15359.
15. Semisotnov, G. V.; Kihara, H.; Kotova, N. V.; Kimura, K.; Amemiya, Y.; Wakabayashi, K.; Serdyuk, I. N.; Timchenko, A. A.; Chiba, K.; Nikaido, K.; Ikura, T.; Kuwajima, K. J Mol Biol 1996, 262, 559–574.
16. Uzawa, T.; Kimura, T.; Ishimori, K.; Morishima, I.; Matsui, T.; Ikeda-Saito, M.; Takahashi, S.; Akiyama, S.; Fujisawa, T. J Mol Biol 2006, 357, 997–1008.
17. Wu, Y.; Kondrashkina, E.; Kayatekin, C.; Matthews, C. R.; Bilsel, O. Proc Natl Acad Sci USA 2008, 105, 13367–13372.
18. Dootz, R.; Otten, A.; Koster, S.; Struth, B.; Pfohl, T. J Phys Condens Matter 2006, 18, S639–S652.
19. Lamb, J. S.; Zoltowski, B. D.; Pabit, S. A.; Crane, B. R.; Pollack, L. J Am Chem Soc 2008, 130, 12226–12227.
20. Das, R.; Kwok, L. W.; Millett, I. S.; Bai, Y.; Mills, T. T.; Jacob, J.; Maskel, G. S.; Seifert, S.; Mochrie, S. G. J.; Thiyagarajan, P.; Doniach, S.; Pollack, L.; Herschlag, D. J. Mol Biol 2003, 332, 311–319.
21. Fang, X. W.; Thiyagarajan, P.; Sosnick, T. R.; Pan, T. Proc Natl Acad Sci USA 2002, 99, 8518–8523.
22. Kwok, L. W.; Shcherbakova, I.; Lamb, J. S.; Park, H. Y.; Andresen, K.; Smith, H.; Brenowitz, M.; Pollack, L. J Mol Biol 2006, 355, 282–293.
23. Roh, J. H.; Guo, L. A.; Kilburn, J. D.; Briber, R. M.; Irving, T.; Woodson, S. A. J Am Chem Soc 2010, 132, 10148–10154.
24. Russell, R.; Millett, I. S.; Doniach, S.; Herschlag, D. Nat Struct Biol 2000, 7, 367–370.
25. Russell, R.; Millett, I. S.; Tate, M. W.; Kwok, L. W.; Nakatani, B.; Gruner, S. M.; Mochrie, S. G. J.; Pande, V.; Doniach, S.; Herschlag, D.; Pollack, L. Proc Natl Acad Sci USA 2002, 99, 4266–4271.
26. Schlatterer, J. C.; Kwok, L. W.; Lamb, J. S.; Park, H. Y.; Andresen, K.; Brenowitz, M.; Pollack, L. J Mol Biol 2008, 379, 859–870.
27. Cech, T. R.; Golden, B. L. In The RNA World; Gesteland, R. F.; Cech, T. R.; Atkins, J. F., Eds.; Cold Spring Harbor Laboratory Press: Cold Spring Harbor, NY, 1998, p 321–349.
28. Zhang, J.; Lau, M. W.; Ferre-D'Amare, A. R. Biochemistry 2010, 49, 9123–9131.
29. Cruz, J. A.; Westhof, E. Cell 2009, 136, 604–609.
30. Williamson, J. R. Curr Opin Struct Biol 2008, 18, 299–304.
31. Svergun, D. I.; Koch, M. H. J Rep Prog Phys 2003, 66, 1735–1782.
32. Fang, X. W.; Littrell, K.; Yang, X.; Henderson, S. J.; Siefert, S.; Thiyagarajan, P.; Pan, T.; Sosnick, T. R. Biochemistry 2000, 39, 11107–11113.
33. Moghaddam, S.; Caliskan, G.; Chauhan, S.; Hyeon, C.; Briber, R. M.; Thirumalai, D.; Woodson, S. A. J Mol Biol 2009, 393, 753–764.
34. Pollack, L.; Doniach, S. In Meth Enzyme: Biophysical, Chemical, and Functional Probes of RNA Structure, Interactions and Folding, Part B; Elsevier Academic Press: San Diego, 2009; Vol. 469, pp 253–268.
35. Chacon, P.; Diaz, J. F.; Moran, F.; Andreu, J. M. J Mol Biol 2000, 299, 1289–1302.

10970282, 2011, 8, Downloaded from https://onlinelibrary.wiley.com/doi/10.1002/bip.21604 by Cornell University, Wiley Online Library on [28/06/2023]. See the Terms and Conditions (https://onlinelibrary.wiley.com/terms-and-conditions) on Wiley Online Library for rules of use; OA articles are governed by the applicable Creative Commons License

36. Heller, W. T.; Abusamhadneh, E.; Finley, N.; Rosevear, P. R.; Trewhella, J. Biochemistry 2002, 41, 15654–15663.
37. Svergun, D. I. Biophys J 1999, 76, 2879–2886.
38. Walther, D.; Cohen, F. E.; Doniach, S. J Appl Crystallogr 2000, 33, 350–363.
39. Lipfert, J.; Doniach, S. Annu Rev Biophys Biomol Struct 2007, 36, 307–327.
40. Lamb, J.; Kwok, L.; Qiu, X. Y.; Andresen, K.; Park, H. Y.; Pollack, L. J Appl Crystallogr 2008, 41, 1046–1052.
41. Treiber, D. K.; Williamson, J. R. Curr Opin Struct Biol 2001, 11, 309–314.
42. Laederach, A.; Shcherbakova, I.; Liang, M. P.; Brenowitz, M.; Altman, R. B. J Mol Biol 2006, 358, 1179–1190.
43. Baird, N. J.; Gong, H. P.; Zaheer, S. S.; Freed, K. F.; Pan, T.; Sosnick, T. R. J Mol Biol 2010, 397, 1298–1306.
44. Solomatin, S. V.; Greenfeld, M.; Chu, S.; Herschlag, D. Nature 2010, 463, 681–684.
45. Cantor, C. R.; Schimmel, P. R. Biophysical Chemistry Part II: Techniques for the Study of Biological Structure and Function; W.H. Freeman: New York, 1980.
46. Knight, J. B.; Vishwanath, A.; Brody, J. P.; Austin, R. H. Phys Rev Lett 1998, 80, 3863–3866.
47. Park, H. Y.; Qiu, X. Y.; Rhoades, E.; Korlach, J.; Kwok, L. W.; Zipfel, W. R.; Webb, W. W.; Pollack, L. Anal Chem 2006, 78, 4465–4473.
48. Sclavi, B.; Sullivan, M.; Chance, M. R.; Brenowitz, M.; Woodson, S. A. Science 1998, 279, 1940–1943.
49. Pabit, S. A.; Qiu, X. Y.; Lamb, J. S.; Li, L.; Meisburger, S. P.; Pollack, L. Nucleic Acids Res 2009, 37, 3887–3896.
50. Bailor, M. H.; Sun, X. Y.; Al-Hashimi, H. M. Science 2010, 327, 202–206.
51. Baird, N. J.; Fang, X. W.; Srividya, N.; Pan, T.; Sosnick, T. R. Q. Rev Biophys 2007, 40, 113–161.
52. Woodson, S. A. Curr Opin Struct Biol 2005, 15, 324–330.
53. Shcherbakova, I.; Brenowitz, M. Nat Protocols 2008, 3, 288–302.
54. Mukhopadhyay, S.; Deniz, A. A. J Fluoresc 2007, 17, 775–783.
55. Walter, N. G.; Harris, D. A.; Pereira, M. J. B.; Rueda, D. Biopolymers 2001, 61, 224–242.
56. Lee, M. K.; Gal, M.; Frydman, L.; Varani, G. Proc Natl Acad Sci USA 2010, 107, 9192–9197.
57. Baird, N. J.; Kulshina, N.; Ferre-D'Amare, A. R. RNA Biol 2010, 7, 328–332.

Reviewing Editor: Sarah A. Woodson

10970282, 2011, 8, Downloaded from https://onlinelibrary.wiley.com/doi/10.1002/bip.21604 by Cornell University, Wiley Online Library on [28/06/2023]. See the Terms and Conditions (https://onlinelibrary.wiley.com/terms-and-conditions) on Wiley Online Library for rules of use; OA articles are governed by the applicable Creative Commons License